SAND2007-0734J

# MOLECULAR DYNAMICS MODELING OF ION ADSORPTION TO THE BASAL SURFACES OF KAOLINITE

Igor F. Vasconcelos, Bruce A. Bunker
*Department of Physics, University of Notre Dame, Notre Dame, IN 46556, USA*

Randall T. Cygan
*Geochemistry Department, Sandia National Laboratories, Albuquerque, NM 87185-0754, USA*

**Abstract**

We used molecular dynamics simulation to study the mechanisms envolved in the adsorption of various ions to the basal surfaces of kaolinite. Analysis of simulation data indicates that cations and anions adsorb preferably on the siloxane and gibbsite surfaces of kaolinite, respectively. We observed strong inner sphere adsorption of chlorine at aluminum vacancies on the gibbsite surface and the occurrence of chlorine-driven inner sphere adsorption of cesium and sodium on the gibbsite surface for high ionic strengths. Cesium ions form strong inner sphere complexes at ditrigonal cavities on the siloxane surface. Outer sphere cesium is highly mobile and only weak adsorption may occur. A small amount of sodium adsorbs on the siloxane surface as inner sphere complexes at not clearly defined sites. Like cesium, sodium onlys forms very weak outer sphere complexes on this surface. Inner sphere complexes of cadmium and lead do not occur on either surface. Relatively strong outer sphere cadmium and lead complexes are present on the siloxane surface at ditrigonal cavities.

## 1 Introduction

The fate of chemical and radioactive wastes, such as radionuclides and heavy metals, in the environment is controlled, to an extended degree, by the ability of subsurface minerals to uptake these contaminants by processes like permanent adsorption and precipitation. Clay minerals are of critical importance on these processes. Because of their great surface reactivity, clays are often able to regulate the composition of soil by adsorbing metals, protons, and organic molecules. They also play an important role on the transport of sorbed contaminants in groundwater.

Clay minerals are abundant in many near-surface geological environments and are highly sorptive due to their small particle sizes, large surface areas, and chemically active surface defect sites. Recognition of the significance of these minerals has recently increased because of the need for environmental remediation. For instance, the reaction of metal cations with mineral surfaces in and near hazardous chemical and radioactive waste sites often controls the fates of these species.

Kaolinite [1, 2, 3, 4] ($Al_2Si_2O_5(OH)_4$) is a 1:1 layer clay composed of a repeating layer of a gibbsite aluminum octahedral sheet and a siloxane silicon tetrahedral sheet. Both layers are connected by bridging oxygens. Each silicon is connected to three other silicon atoms by bridging oxygens forming the siloxane surface. This arrangement of tetrahedral silicons give rise to hexagonal cavities on the surface. In the gibbsite sheet, each aluminum is coordinated by two oxygens of the siloxane sheet and shares four hydroxyls with neighboring aluminum atoms. Three of these hydroxyls are oriented towards the external surface forming the gibbsite surface while the fourth one is oriented inwards in the direction of the siloxane cavity [5]. This layered structure extends to edges of the crystal where exposed dangling silicon and aluminum atoms are terminated by hydroxyls.

The ion retention capabilities of kaolinite is known to be low with respect to smectites and illites and most of the long term adsorption is due to the presence of impurities [6]. However, kaolinite is of interest because important nuclear sites are located on kaolinite-rich soils and even a minute retention capacity would be important if the issues were the migration of a contaminants over distances measured in kilometers. Furthermore, kaolinite provides a relatively simple substrate for studying surface adsorption due to its lack of interlayer metal sites and the presence of both hydrophilic and hydrophobic basal surfaces, which makes it an attractive object of study.

Adsorption on clay minerals can occur via two mechanisms: outer-sphere adsorption, which occurs primarily on the basal planes existing in the outside surfaces and interlayer regions of clays minerals, and inner-sphere adsorption, which occurs at the silicon hydroxyls (silanols) and aluminum hydroxyls (aluminols) existing on the edge of clay minerals [7, 8]. It is known that the adsorption mechanisms are different for different metal cations and therefore individual studies are required.

In this paper, we study the structure and dynamics of adsorbed $Cs^+$, $Na^+$, $Cd^{+2}$, and $Cd^{+2}$ in the mineral/aqueous solution interface at the basal surfaces of kaolinite. Cesium, cadmium,and lead and of great interest in environmental science applications due to their toxic nature. Sodium, on its turn, is a very common ion in background electrolytes and hence the importance to understand its role on adsorption processes.

Cadmium and lead are highly toxic elements that can pollute water and soils due to their numerous uses. Adsorption of cadmium and lead from clay particles largely determine their availability within the environment and it has been the subject of many studies over the years [9, 10, 8, 11, 12, 13] (cadmium) and [9, 14, 15, 16] (lead).

The interaction between cadmium and lead and kaolinite surfaces can be summarized as follows: adsorption isotherms [17] indicate that cadmium adsorbs very little to kaolinite at pH $< 7$. At pH 8, adsorption began to increase rapidly and at pH 9 most of the cadmium is adsorbed to the kaolinite surface. Adsorption isotherms also indicate a small percentage of lead adsorbed to kaolinite between pH 4.5 and 6. At pH $> 6$, adsorption begins to increase until pH 8 at which point most of the lead is adsorbed to the kaolinite surface. The low adsorption in acidic conditions can be explained by the competition between protons and metallic cations for the edge aluminols and silanols leaving the basal surfaces as the primary destination for the cations.

$^{137}Cs$ is an important component of nuclear waste and its storage and migration in natural environments have been studied by many investigators [18, 19, 20, 21, 22, 23, 24, 25, 26]. $^{137}Cs$ has been introduced to soils and groundwater over the past five decades by nuclear accidents, as fallout from nuclear testing, and as a byproduct of nuclear research and weapons production. Measurements of relative adsorption as a function of pH (adsorption isotherms) [20] suggest a pH-dependent affinity of $Cs^+$ for the Al octahedral edge sites of the crystal and only a possible weak binding on the tetrahedral Si edge site at high pH values. Adsorption on the basal surfaces appears

to be pH-independent. There appears to be a significant pH-independent amount of adsorption indicating a stronger interaction of cesium with the basal surfaces of kaolinite as opposed to cadmium and lead.

## 2 The Model

We use the CLAYFF forcefield [5] to model kaolinite and its interface aqueous solutions of CsCl, NaCl, $CdCl_2$, and $PbCl_2$. CLAYFF has been used successfully to obtain structural and dynamical properties of hydrated mineral systems and their interfaces with aqueous solutions [27, 28]. One of the key features of CLAYFF is its flexibility within the clay lattice where the metal-oxygen interactions are described by a 12-6 Lennard-Jones term and a Coulombic function with partial charges derived by quantum chemistry methods [29]. The only bonded interactions are those within water molecules (bond stretch and angle bend) and hydroxyls (bond stretch) based on the SPC water model [30], which has been used to study properties of bulk water and aqueous systems [30, 31, 32, 33]. The SPC water model is relatively simple and has partial charges centered directly on each of the three atoms. Tables 1 and 2 show the forcefield parameters for all nonbonded and bonded interactions, respectively.

Kaolinite ($Al_2Si_2O_5(OH)_4$) is a 1:1 layer clay composed of a layer made up of a $AlO_6$ octahedral sheet and a $SiO_4$ tetrahedral sheet. Layers are kept together by hydrogen bonds between hydroxyl groups extending from the octahedral surface of a layer and basal oxygens on the tetrahedral surface of the next layer. For the present work, we use equilibrated, neutral kaolinite structures as those obtained in ref. [5], converted into orthogonal cells oriented in a such way that the (001) and $(00\bar{1})$ planes correspond to the octahedral and tetrahedral basal surfaces, respectively.

The simulation cells we use contain 243 kaolinite unit cells ($9 \times 9 \times 3$ units in the $a$, $b$, and $c$ dimensions) with a total of 8262 atoms in the solid. The corresponding $a$ and $b$ dimensions are 46.5 Å and 80.3 Å and are fixed over all the simulations. The kaolinite crystal and solution are charge neutral, making our results pH independent. The basal surface of kaolinite controls adsorption at lower pHs, while at higher pHs the edge sites are expected to be dominant.

To simulate the solid/liquid interface, we bring an aqueous region of dimensions 46.5 Å $\times$ 80.3 Å $\times$ 35.4 Å with 3600 water molecules in contact with one of the basal surfaces of kaolinite to create the initial crystal-aqueous

solution cell with $c$ dimension of 57.1 Å . We impose periodic boundary conditions on the three dimensions so that both basal surfaces are in contact with the solution, and run short NPT simulations (with only the $c$ dimension allowed to vary) to equilibrate the solid/liquid interfaces. Kaolinite is a unique mineral because both (001) and $(00\bar{1})$ surfaces are exposed to the aqueous solution and molecular dynamics simulations provide an opportunity to examine both surfaces simultaneously, and that direct comparisons can be made from results

Finally, we insert 7, 32, and 64 cations (and the required number of $Cl^-$ anions to ensure charge neutrality) in the solution to create 0.1 M, 0.5 M, and 1.0 M solutions for each of the 4 cations studied. The ions are randomly inserted just a few angstroms from the midplane of the aqueous region to avoid biased adsorption. We then run a few picoseconds of NPT dynamics to equilibrate the water structure around the added ions.

We use Materials Studio software (Accelrys, Inc., San Diego, CA) to create the simulation cells and to visualize the results and the LAMMPS (Large-scale Atomic/Molecular Massively Parallel Simulator) program [34] on a parallel Linux cluster to run all the simulations. We use the constant NPT [35, 36] (number of atoms, pressure 0 atm, and temperature 300 K) with only the $c$ dimension allowed to vary and constant NVT [37, 38] (number of atoms, volume, and temperature 300 K) ensembles with barostat and thermostat relaxations times of 100 fs and 500 fs, respectively. The equations of motion were integrated using Verlet's algorithm [39, 40] with time steps of 1 fs. We use the Ewald summation method [41] to calculate long-range electrostatic interactions.

We used a total of 12 (4 cations and 3 concentrations) of the optimized structures described above (a typical structure is shown in Figure 1(a)) containing about 19000 atoms each as starting configurations for the molecular dynamics simulations presented in this study. In a typical simulations, we first let the $c$ dimension relax for a period of 100 ps of NPT dynamics. To ensure equilibrium of the adsorption dynamics, we simulate (NVT) for an extra 500 ps. We finally record the equilibrium dynamic trajectory for each model for statistical analysis at 100 fs intervals during the next 500 ps of NVT dynamics to provide 5000 trajectory frames

To analyze the results obtained from the various simulations, we calculate radial distribution functions [42] and atomic density profiles [27, 28] in the [001] direction perpendicular to the solid/liquid interface ($c$ dimension). We also calculate atomic density maps [27] within planes parallel to

the solid/liquid interfaces at characteristic distances to the surfaces for each atomic type involved in the adsorption processes.

## 3 Results and Discussions

Figure 1(a) shows the initial configuration of a 0.5 M CsCl solution in contact with the basal surfaces of kaolinite. A typical simulation starts from a structure similar to this. After just a few picoseconds, cations and anions difuse preferentially toward the $SiO_4$ tetrahedral and $AlO_6$ octahedral surfaces, respectively. We also observe that the $c$ dimension of the cell does not change during the last 50 ps indicating that the volume of the solution reached an equilibrium value.

Figure 1(b,c) shows graphical representations of the 0.5 M CsCl simulation cell after 100 ps and 600 ps of dynamics. We can see a similar distribution of ions along the $c$ axis in both structures, indicating that equilibrium is reached within that initial period of 100 ps. Stabilization of potential energy values (not shown) confirms equilibration after the 600 ps period. The pattern observed for other concentrations and other cations is consistent with this picture.

To investigate the adsorption processes as function of ions loading, we work with three concentrations (0.1 M, 0.5 M, and 1.0 M) of CsCl, NaCl, $CdCl_2$, and $PbCl_2$. Figure 2 shows 0.1 M, 0.5 M, and 1.0 M CsCl and $CdCl_2$ solutions in equilibrium with the basal surfaces of kaolinite, after 600 ps. At lower ionic strengths (0.1 M), the solutions are far from saturation and there is a complete separation between cations and anions with virtually all ions associated with either surface (Figure 2-top two pictures). $Cs^+$ ions lose part of their hydration shell to come very close to the surface in an inner sphere like adsorption, while the presence of a layer of water between $Cd^{+2}$ ions and the surface suggests that $Cd^{+2}$ ions retain the structure of their bulk solution hydration shells forming what looks like outer sphere adsorption complexes (see Figure 4). It suggests strong and weak affinity between $Cs^+$ and $Cd^{+2}$, respectively, and the mineral surfaces. We will discuss these issues in details later on. It is important to point out the contrast in water disposition immediately at the interfaces. The siloxane is relatively hydrophobic while the gibbsite surface (and hydroxyls) is hydrophyllic and has significant hydrogen bonding. The flexible and unconstrained CLAYFF accurately models this type of behavior.

With increase in ionic strength, and consequent approach of saturation,

there is an increasing number of ions remaining in the bulk solution. At 1.0 M, most of the ions are found in the bulk solution (Figure 2-bottom two pictures, Figure 3) forming a structure similar to the original solution. Also at 1.0 M, we notice the presence of some $Cs^+$ and $Na^+$ ions close to the $AlO_6$ octahedral surface. Most of these ions are paired with a $Cl^-$ ion suggesting a $Cl^-$ driven adsorption of $Cs^+$ and $Na^+$ on the octahedral basal surface. The same, however, does not happen with $Cd^{+2}$ and $Pb^{+2}$ ions.

Before proceeding with further discussion, we shall define inner sphere and outer sphere adsorption in the scope of this work. An ion forms an inner sphere adsorption complex if it is found, in equilibrium, at a distance of $\sim$2.5 Å to $\sim$3.0 Å from a surface, with no water molecules between the metal and the surface, and has little mobility in the plane parallel to the surface, for a long enough period of simulation (500 ps). The same applies for the outer sphere, except the distances are $\sim$2.0-2.5 Å beyond those of inner sphere's. Outer sphere adsorption is also characterized by the presence of an intermediate water molecule between the metal and the surface.

Looking at the configurations of 1.0 M CsCl, NaCl, $CdCl_2$, and $PbCl_2$ solutions in equilibrium with kaolinite in Figure 3, we can make some inferences with respect to the adsorption processes. Adsaorption mechanisms on the $AlO_6$ octahedral surface are mostly unchanged for the various cations and concentrations (except for the little $Cl^-$ driven dsorption of $Cs^+$ and $Na^+$) and therefore will not be the focus of our discussion.

We find that like $Cd^{+2}$, $Pb^{+2}$ forms complexes consistent with outer sphere adsorption on the tetrahedral $SiO_4$ surface. So does $Na^+$ with the exception of a few ions found at distances to the surface consistent with inner sphere adsorption. However, as we will see later on, $Na^+$ ions have great mobility parallel to the mineral surface and fall outside our definition of adsorption. $Cs^+$ appears to adsorb as outer sphere complexes as well but, very much like $Na^+$, these are very short-alived complexes and could hardly be regarded as adsorbed. Figure 4 shows an equilibrium configuration of mineral-solution interface at the $SiO_4$ tetrahedral surface for better visualization of these points.

We have so far assumed that the configurations shown in the previous figures are representative of the steady-state equilibrium of the mineral-solution interfaces. To validate (or negate) assumptions made above, we need to extend the analysis beyond what can be inferred from assumed representative configurations. We use atomic density profiles and atomic trajectory maps to achieve this goal.

### 3.1 Atomic Density Profiles

An atomic density profile [27, 28] $\rho_i(z)$ is a measure of the probability of finding an atom of type $i$ along the $c$ axis, at distance $z$ from a fixed origin. We calculate density profiles by averaging the trajectories of each atomic species during 500 ps following the equilibration period. The integral of $\rho_i(z)$ over a certain rage $\Delta z$ gives the total number of species $i$ atoms in the slab of area $a \times b$ and thickness $\Delta z$. Density profiles are a very effective tool to describe interfaces.

Figure 5 shows atomic density profiles for the three concentrations of CsCl solution in equilibrium with kaolinite. Regions 1 and 2 in the picture correspond to our definition of inner and outer sphere ranges given above. Water molecules in regions 1 at both surfaces form hydrogen bonds with oxygen/hydrogen atoms on either surface and are therefore strongly oriented. The presence of the surfaces affects the orientation of water molecules up to about 10 Å from either surface, from which point they are randomly oriented as expected in bulk water [27]. This orientation of water molecules is not affected by the presence of ions in solutions.

The left hand side surface of Figure 6 represents the octahedral $AlO_6$ surface with the Al-bonded hydroxyls sticking out. The slightly positively-charged surface attracts $Cl^-$ ions. The reasonably narrow peak in the $Cl^-$ density profile inside the inner sphere region suggests a fairly strong interaction between $Cl^-$ and the surface. This is confirmed by the distinct presence of a second and a third (for 0.5 M and 1.0 M solutions) layers of $Cl^-$. The mechanism for $Cl^-$ adsorption on this surface appears to be fairly concentration independent. Increasing height of peaks at inner and outer sphere distances with increasing concentration indicates a correlation between number of anions apparently adsorbed and number of anions present in solution. Long lived presence of some $Cs^+$ inside the inner sphere region for the 1.0 M case reinforces the $Cl^-$ driven $Cs^+$ adsorption and ion pairing mechanism. Ion pairing is negligible for 0.5 M and nonexistent for 0.1 M.

At the opposite kaolinite surface, Si-bridging oxygen atoms relax outward slightly with respect to the silicon atoms and the surface has thus a very small net negative charge, which drives $Cs^+$ ions towards it. The inner shell $Cs^+$ peak is significantly wider (it is actually a superposition of two very closely spaced peaks) than the $Cl^-$ peak, which is a consequence of the large size and soft electron structure of $Cs^+$, in the sense that it does not usually bind strongly. At 0.1 M almost all the cations are found within the inner sphere

distance, as we suggested above, while at higher concentrations, some $Cs^+$ is also found in the outer sphere region. Peaks consistent with inner sphere $Cs^+$ at concentrations of 0.5 M and 1.0 M are comparable in height with a little increase in the height of the more distant peak for the 1.0 M case, indicating that saturation is close to being achieved.

Figure 6 shows the atomic density profiles for 0.5 M CsCl, NaCl, $CdCl_2$, and $PbCl_2$ solutions in contact with kaolinite. Most of $Cd^{+2}$, $Pb^{+2}$, and $Na^+$ ions are found at a distance to the surface consistent with outer sphere adsorption, for the duration of the 500 ps period. The tail of the $Na^+$ peak leaks in the inner sphere range suggesting some $Na^+$ inner sphere adsorption, consistent with the inference we made above based on the snapshot configurations.

In order to quantify the information inferred from the atomic density profiles like those in Figure 5 and Figure 6, we integrate the various ions profiles over the inner sphere and inner+outer sphere regions to obtain the adsorption statistics shown in Table 3. The columns are as follows: $N_{tot}$ is the total number of that particular ion in the system; $N_{ad}$ is the number of ions within a particular region (inner sphere or total); $X_{ad}$ is the percentage of the total number of ions $N_{ad}$ represents; and $\rho$ is the number of ions per unit surface area, in units of $1/nm^2$. $\rho$ is equivalent to adsorption site density.

Adsorption of $Cl^-$ on the $AlO_6$ surface is affected by the type of cation present in solution. $Cd^{+2}$ and $Pb^{+2}$ seem to affect $Cl^-$ adsorption in a similar way, resulting in consistent numbers in Table 3 for the all the three concentrations of $CdCl_2$ and $PbCl_2$. Numbers are also consistent for 0.1 M CsCl and NaCl solutions. However, for increasing ionic strengths, $Cs^+$ and $Na^+$ affect $Cl^-$ adsorption in a different way. At 0.5 M, the amount of inner sphere adsorption of $Cl^-$ is virtually the same ($\rho = 0.29$ sites/$nm^2$) in the presence of both cations while outer sphere adsorption is a little inhibited by the presence of $Cs^+$ ($\rho = 0.18$ sites/$nm^2$ as opposed to 0.26 sites/$nm^2$ in the presence of $Na^+$). At 1.0 M, both inner and outer sphere $Cl^-$ adsorption is inhibited in the presence of $Cs^+$ (see table). We attribute this process to the formation of ions pairs close to the surface: a $Cs^+$ ion is signficantly larger than a $Na^+$ ion (1.69 Å vs. 0.95 Å) and tends to occupy space $Cl^-$ ions would be found in a more significant way than $Na^+$. This effect becomes more important with increasing number of ion pairs formed and with approach to saturations.

The valence of cations also seems to play a role on $Cl^-$ adsorption. The loading of $Cl^-$ on the surface for the same number of anions present in solution is consistently lower for divalent cations as it is for monovalent ones. We

attribute this difference to the stronger interaction between $Cl^-$ anions and divalent cations. Site densities are roughly 0.50 sites/nm$^2$ as inner sphere and 0.80 sites/nm$^2$ total at the highest load of $Na^+$ and both divalent cations, indicating that saturation of $Cl^-$ on the $AlO_4$ surface is reached.

At the opposite kaolinite surface, we find inner sphere site densities for $Cs^+$ to be 0.35 and 0.38 site/nm$^2$ for 0.5 M and 1.0 M solutions, respectively, indicating saturation of $Cs^+$ adsorption sites on the surface. These numbers include the little $Cl^-$-driven adsorption of $Cs^+$ on the $AlO_4$ surface which account for just a negligible fraction of the toal. In the same way, we find saturation densities of 0.35-0.38 sites/nm$^2$ for $Pb^{+2}$ and 0.30 sites/nm$^2$ for $Cd^{+2}$, revealing that $Pb^{+2}$ has a slightly larger affinity to the surface than $Cd^{+2}$. As expected, no $Cd^{+2}$ or $Pb^{+2}$ is found within inner sphere range for this surface. We also observe less than 1 $Na^+$ at inner sphere distance regardless of the the number of ions in solution, and unlike $Cs^+$, a considerable fraction of this already small amount is due to adsorption on the $AlO_4$ surface.

### 3.2 Trajectory maps

A trajectory map [27] is simply a map of the integrated atomic motions of chosen atomic types over the 500 ps of accumulated trajectories. We select slices along the $c$ axis located at positions $_i$ and with thicknesses $dz_i$ and map trajectories of the atoms onto a grid in the $a-b$ plane. In our discussions, $z_i$ and $dz_i$ are always defined as the inner and outer sphere ranges defined above at the solid-liquid interfaces.

Figure 7 shows the trajectories of $Cs^+$ ions within inner (a) and outer (b) spheres ranges from the $SiO_4$ surface, superimposed on the trajectories of silicon and bridging oxygen atoms on the outermost layer of kaolinite. The trajectories indicate that inner sphere $Cs^+$ ions are found preferentially over the hexagonal cavities on the surface, and have little mobility beyond the center of the cavity. Outer sphere trajectories, on the other hand, are quite difuse over the whole surface with little indication of long-lived complex formation.

Unlike $Cs^+$ ions within inner sphere distances from the $SiO_4$ surface, the few inner sphere $Na^+$ ions are not consistently found in what seems to be an equilibrium adsorption site, as we can see in Figure 8(a). Outer sphere $Na^+$ ions, like $Cs^+$ in the same situation, are quite mobile on the $a-b$ plane with no formation of stable long-lived complexes (see Figure 8(b)).

Figure 9 shows trajectory maps of (a) $Cd^{+2}$ and (b) $Pb^{+2}$ ions within outer sphere distances from the $SiO_4$ surface. We have seen above that these ions are not found inside the inner sphere region for this surface. It is clear from the trajectory maps that both $Cd^{+2}$ and $Pb^{+2}$ cations are mostly found on the hexagonal cavities on the surface, just like the inner sphere $Cs^+$ ions. The trajectories are not so tightly concentrated around the centers of the cavities as the inner sphere $Cs^+$ ones, indicating that these complexes are not quite as stable, which is not surprising considering the longer distance and the presence of water molecules between the cations and the surface.

Figure 10 shows the trajectories for 1.0 M CsCl solution in contact with the $AlO_4$ surface. $Cl^-$ anions clearly adsorb as inner sphere complexes above the aluminum vacancy and are coordinated by three oriented hydroxyls. Inner sphere $Cs^+$ complexes also occur, almost always coordinated as an ior pair with $Cl^-$. $Na^+$-$Cl^-$ pair formation also occurs while $Pb^{+2}$-$Cl^-$ and $Cd^{+2}$-$Cl^-$ pairs do not (not shown). Outer sphere $Cl^-$ trajectories are more diffuse indicating weaker adsorption, as expected for outer sphere complexes.

### 3.3 Radial distribution functions and structural information about adsorption sites

Before we proceed with further discussion of these results, we shall summarize our findings so far. On the $AlO_6$ octahedral surface, we found strong $Cl^-$ inner sphere adsorption above aluminum vacancies and weak outer sphere adsorption. We also identify formation of inner sphere $Cs^+$-$Cl^-$ and $Na^+$-$Cl^-$ complexes. $Cl^-$-controlled adsorption of $Cd^{+2}$ and $Pb^{+2}$ does not occur.

Regarding the $SiO_4$ tetrahedral surface, we identified a fairly strong adsorption of $Cs^+$ as inner sphere associated with the hexagonal cavities. Despite the presence of a peak in the $Cs^+$ density profile consistent with outer sphere asorption, the diffuse trajectories indicate very weak adsorption. Similar reasoning applies to outer sphere $Na^+$ ions. Inner sphere $Na^+$ complex formation also occurs although not necessarily at a fixed site. No $Cd^{+2}$ and $Pb^{+2}$ are found inside inner sphere region. However, fairly stable and long-lived outer sphere $Cd^{+2}$ and $Pb^{+2}$ complexes exist, confirmed by both atomic density profile and trajectory maps. Like inner sphere $Cs^+$ complexes, outer sphere $Cd^{+2}$ and $Pb^{+2}$ complexes adsorb at the hexagonal cavity.

Table 4 shows values of solvation and inner sphere adsorption (on the $SiO_4$ surface) energies for the various cations. The solvation energy is the energy associated with a fully hydrated ion and is calculated as the energy

difference between the solvated ion and that of the solvent. The inner sphere adsorption energy is defined here as the energy associated with an inner sphere adsorption complex and is calculated by taking the energy difference between a solution-mineral system with aa cation adsorbed at a surface hexagonal cavity as an inner sphere complex and that of the same system without the cation present.

The solvation energy is a measure of the energetic penalty associated with separating an ion from its hydration shell, while the inner sphere adsorption energy is the energy it takes to remove from the system an ion that is sorbed at a hexagonal cavity. Comparing these two energies for the same type of ion gives us a measure of how energetically favorable/unfavorable it is to take an ion from the bulk solution and form an inner sphere adsorption complex, and vice versa.

Because $Cs^+$ has a very large ionic size and charge of just +1, the water molecules of its hydration shell are not very tightly bound. There is a fairly large amount of water molecule exchange between the hydration shell and the bulk solution. As a consequence, the solvation and inner sphere adsorption energies of $Cs^+$ in Table 4 are such that it is energetically favorable for $Cs^+$ to lose part of its hydration sphere and adsorb directly to the surface as an inner sphere complex, despite its weak interaction with the surface.

$Na^+$ ions are considerably smaller than $Cs^+$ ions and so have a slightly larger (more negative) solvation energy than $Cs^+$ (see Table 4) and therefore the water molecules are more strongly bound to $Na^+$ than to $Cs^+$. The solvation energy of $Na^+$ is just a little more negative than its inner sphere adsorption energy (see Table 4) indicating that it is not so favorable for $Na^+$ to adsorb directly to the surface at the expense of a fewer water molecules on its hydration shell. However, the energy difference does allow for a few $Na^+$ ions to get close to the surface.

$Cd^{+2}$ and $Pb^{+2}$ have, on their turn, a charge of +2 and interact more strongly with the water molecules, keeping them tightly bound on a fairly stable hydration shell. It is very costly energetically to remove water molecules from the hydration shells of the cations and as a consequence, no $Cd^{+2}$ or $Pb^{+2}$ can be found inside the inner sphere regions. The electrostatic interaction between the divalent $Cd^{+2}$ and $Pb^{+2}$ is still strong enough to keep the hydrated cation adsorbed as outer sphere complexes. Such interaction is not strong enough for the monovalent $Cs^+$ and $Na^+$ to form stable outer sphere adsorption complexes, and that explains the diffuse trajectories.

We use radial distribution functions (RDF) [42] to characterize the struc-

ture of adsorption sites on the $SiO_4$ surface. An RDF, $g_{ij}(r)$, is the simplest one of a set of correlation functions between particles. It translates the probability, averaged over time, of finding a pair of atoms of types $i$ and $j$ separated by a distance between $r$ and $r + \delta r$ ($\delta r$ is a small number), with respect to the probability expected from a completely random distribution of particles with the same density. The existence of a coordinated shell of atoms of type $j$ at a certain distance around atoms of type $i$ is manifested by the presence of a peak in the RDF centered at a position corresponding to this distance. The average number of atoms in this shell is given by the area under the peak and is obtained by integrating $g_{ij}(r)$ from immediately before to immediately after the peak. We typically chose the positions at the minima of the curve that precede and follow as the limits of this peak, or just a point where the RDF is zero when this is the case.

Figure 11(a) shows RDFs with $Cs^+$ ions in the central position calculated from am equilibrated 0.1 M CsCl solution in contact with kaolinite averaged over 500 ps. Only inner sphere cations are included in the calculations. Cs-O*, Cs-Ob, and Cs-Si RDFs correspond to the configuration of water oxygen (O*), bridging oxygen (Ob), and silicon (Si) atoms, respectively, around the aforementioned $Cs^+$ ions. The graph in the detail shows the average number of atoms of these three species as a function of distance to the central cation, along with the Cs-O* number of atoms curve calculated from $Cs^+$ solvated in bulk water. A graphical representation of a typical adsorption complex on the $a-b$ plane (top) and along the $c$ axis (bottom) is shown in Figure 11(b).

The Cs-O* RDF presents a pronounced peak corresponding to a first hydration shell, and a diffuse peak for the second shell. The absence of a clear separation between first and second hydration shells is a consequence of the weak interaction between $Cs^+$ and water molecules we mentioned above. This peak is defined between 2 Å and roughly 3.9 Å and is centered at $\approx$ 3.12 Å. The uncertainty in this distance is estimated as the half-width at half-height of the peak and is $\approx$ 0.25 Å. The number of water molecules in the first hydration shell is obtained from the corresponding N(R) curve at a distance R$\approx$3.9 Å. The coordination number of the first hydration shell of $Cs^+$ decreases from 8.3 for the solvated ion to 5.6 for the adsorbed ion. The distance of 3.12 Å remains unchanged. All distances, coordination numbers and uncertainties given in the following are obtained in this same fashion.

Cs-Ob and Cs-Si RDFs, on the other hand, have several peaks up to large distances as we expect from the crystal structure of the substrate. The first peak in each of Cs-Ob and Cs-Si RDFs corresponds to 5.1 Ob atoms and 5.4

Si atoms distant 3.42 Å and 4.06 Å to the $Cs^+$ ion. This picture is consistent with inner sphere adsorption on a cavity formed by the Ob and Si hexagonal lattices rotated by 30° with respect to each other (Figure 11(b)).

Figure 12 shows aqueous and sorbed Cd-O* RDFs along with the average number of atoms as a function of distance to the central atom. We do not show $Pb^{+2}$ g(R) and N(R) but the behavior is very similar to that of $Cd^{+2}$ and the analysis follows in the same way. Cations in the bulk solution are left out of the adsorbed Cd-O* and Pb-O* calculations to assure that we isolate the structure of outer sphere adsorption complexes. Bulk solution and adsorbed Cd-O* and Pb-O* (not shown) RDFs present the same first shell of oxygen atoms with the same coordination numbers of 7.0 and 8.4 and distances of 2.31 Å and 2.65 Å for $Cd^{+2}$ and $Pb^{+2}$, respectively. This indicates that the first hydration shell remains unchanged. The presence of the surface makes the second hydration shells of adsorbed complexes to have about 2.5 to 3 fewer water molecules, in average, than aqueous complexes. Cd-Ob (Figure 13(a)) and Pb-Ob (not shown) RDFs are very diffuse without a sharp separation between the first shell and the remaining Ob atoms in the substrate crystal. We can, nevertheless, clearly identify the presence of a defined shell centered at about 5.1 Å, for $Cd^{+2}$ and 5.4 Å, for $Pb^{+2}$ with 5-7 atoms in it. This description is consistent with a fully hydrated $Cd^{+2}$ ions adsorbed on a hexagonal cavity on the surface.

The hydration shells of $Na^+$ in the bulk water and within adsorption distance from the surface follow very closely the ones of $Cd^{+2}$ and $Pb^{+2}$. The first shell is virtually unchanged while the second shell loses about three water molecules (not shown). The coordination of $Na^+$ with the surface, however, does not follow that of $Cd^{+2}$ and $Pb^{+2}$, as we can see in the Na-Ob and Na-Si in Figure 14. The sharp peaks between 2 Å and 4 Å correspond to the few $Na^+$ ions found within inner sphere range as we pointed out previously. Coordination numbers of less than 1 are consistent with $Na^+$ staying directly above either a Si or an Ob atom rather than the hexagonal cavity. Moreover, the absence of clear coordination shells beyond those just mentioned in either Na-Ob and Na-Si confirms the suggestion of high mobility of $Na^+$ ions within outer sphere distance and absence of strongly bound adsorption sites.

Table 5 summarizes all the structural parameters for aqueous and adsorbed complexes calculated from RDFs along with reference numbers obtained from the literature. Our parameters for the hydration shell of aqueous $Cs^+$ are in very good agreement with those obtained from experiments and other simulations. So are the parameters for $Pb^{+2}$ first hydration shell.

Cd-O* distances for both the first and second hydration shells are in good agreement with experimental results, while the coordination numbers are in slight disagreement. We find a first shell coordination number of 7 while it is consistently reported as 6. The second shell coordination number we find is more than 2 lower than what is reported, even after we account for the uncertainty of our calculations. Coordination numbers and distance for aqueous Na-O* are in reasonable agreement with results from both experiments and other molecular modeling simulations.

## 4 Conclusions

We used molecular dynamics simulations to study the interaction between aqueous ions and the basal surfaces of kaolinite. The pair interaction between atoms in the system was modeled using the CLAYFF forcefield. CLAYFF is very flexible (the only bonded interactions are within water molecules and hydroxyls) successfully models mineral/aqueous solution interfaces, as we confirmed in this study.

We studied kaolinite and its interface with aqueous solutions of CsCl, NaCl, $CdCl_2$, and $PbCl_2$ at concentrations of 0.1 M, 0.5 M, and 1.0 M. Analysis of simulation data indicates that cations and anions adsorb preferably on the siloxane and gibbsite surfaces of kaolinite, respectively. We observed strong inner sphere adsorption of chlorine at aluminum vacancies on the gibbsite surface and the occurrence of chlorine-driven inner sphere adsorption of cesium and sodium on the gibbsite surface for high ionic strengths. Cesium ions form strong inner sphere complexes at ditrigonal cavities on the siloxane surface. Outer sphere cesium is highly mobile and only weak adsorption may occur. A small amount of sodium adsorbs on the siloxane surface as inner sphere complexes at not clearly defined sites. Like cesium, sodium only forms very weak outer sphere complexes on this surface. Inner sphere complexes of cadmium and lead do not occur on either surface. Relatively strong outer sphere cadmium and lead complexes are present on the siloxane surface at ditrigonal cavities. Calculated solvation and inner sphere adsorption (on the siloxane surface) energies for the various cations helps understand the behavior of adsorbed ions on this surface. Structural parameters such as coordination numbers and characteristic distances obtained from radial distribution functions are mostly in agreement with experimental and molecular modeling results published in the literature.

## 5 Acknowledgements

The authors acknowledge the U. S. Department of Energy, Office of Basic Energy Sciences for financial support through the Environmental Molecular Science Institute program. Sandia is a multiprogram laboratory operated by Sandia Corporation, a Lockheed Martin Company for the United States Department of Energy's National Nuclear Security Administration under contract DE-AC04-94AL85000.

**References and Notes**


(1) Brady, P. V.; Cygan, R. T.; Nagy, K. L *J. Colloid. Interface Sci.* **1996**, 183, 356.

(2) Huertas, F. J.; Chou, L.; Wollast, R. *Geochim. Cosmochim. Acta* **1998**, 62, 417.

(3) Sutheimer, S. H.; Maurice, P. A.; Zhou, Q. H. *Amer. Mineralogist* **1999**, 84, 620.

(4) Ganor, J; Cama, J.; Metz, V. *J. Colloid. Interface Sci.* **2003**, 264, 67.

(5) Cygan, R. T.; Liang, J. J.; Kalinichev, A. G. *J. Phys. Chem. B* **2004**, 108, 1255.

(6) Kim, Y.; Cygan, R. T.; Kirkpatrick, R. J. *Geochim. Cosmochim. Acta* **1996**, 60, 1041.

(7) Sposito G. *Rev. Mineral.* **1990**, 23, 261.

(8) Spark, K. M.; Wells, J. D.; Johnson, B. B. *European J. Soil Sci.* **1995**, 46, 633.

(9) Forbes, E. A.; Posner, A. M.; Quirk, J. P. *J. Soil Sci.* **1976**, 27, 154.

(10) Schindler, P. W.; Liechti, P.; Westall J. C. *Neth. J. Agric. Sci.* **1987**, 35, 219.

(11) Angove, M. J.; Johnson, B. B.; Wells, J. D. *Colloids Surfaces A* **1997**, 126, 137.

(12) Angove, M. J.; Johnson, B. B.; Wells, J. D. *J. Colloid. Interface Sci.* **1998**, 204, 93.

(13) Echeverria J. C.; Churio E.; Garrido J. J. *Clay. Clay Miner.* **2002**, 50, 614.

(14) Reed, B. E.; Carriere, P. C.; Moore, R. *J. Env. Eng.* **1996**, 122, 48.

(15) Ikhsan, J.; Johnson, B. B.; Wells, J. D. *J. Colloid. Interface Sci.* **1999**, 217, 403.

(16) Strawn, D. G.; Sparks, D. L. *J. Colloid. Interface Sci.* **1999**, 216, 257.

(17) Hepinstall, S. E.; Turner, B. F.; Maurice, P. A. *Clay. Clay Miner.* **2005**, 53, 557.

(18) Komarneni, S. *Soil Sci. Soc. Am. J.* **1978**, 42, 531.

(19) Evans, D. W.; Albers, J. J.; Clark III, R. A. *Geochim. Cosmochim. Acta* **1983**, 47, 1041.

(20) Westrich, H. R.; Cygan, R. T.; Brady, P. V.; Nagy, K. L.; Anderson, H. L.; Kim, Y.; Fitzpatrick, R. J. The Sorption Behavior of Cs and Cd onto Oxide and Clay Surfaces. In *Proceedings of the waste management conference, WM'95*

(21) Kim, Y.; Kirkpatrick, R. J.; Cygan, R. T. *Geochim. Cosmochim. Acta* **1996**, 60, 4059.

(22) Kemner, K. M.; Hunter, D. B.; Bertsch, P. M.; Kirkland, J. P.; Elam, W. T. *J. Physique IV* **1997**, 7, 777.

(23) McKinley, J. P.; Zachara, J. M.; Heald, S. M.; Dohnalkova, A.; Newville, M. G.; Sutton, S. R. *Environ. Sci. Technol.* **2004**, 38, 1017.

(24) Bostick, B. C.; Vairavamurthy, M. A.; Karthikeyan, K. G.; Chorover, J. *Environ. Sci. Technol.* **2002**, 36, 2670.

(25) Zachara, J. M.; Smith, S. C.; Liu, C. X.; McKinley, J. P.; Serne, R. J.; Gassman, P. L. *Geochim. Cosmochim. Acta* **2002**, 66, 193.

(26) Nakano, M.; Kawamura, K.; Ichikawa, Y. *Appl. Clay Sci.* **2003**, 23, 15.

(27) Wang, J.; Kalinichev, A. G.; Kirkpatrick, R. J.; Cygan, R. T. *J. Phys. Chem. B* **2005**, 109, 15893.

(28) Greathouse, J. A.; Cygan, R. T. *Phys. Chem. Chem. Phys.* **2005**, 7, 3580.

(29) Payne, M. C.; Teter, M. P.; Allan, D. C.; Arias, T. A.; Joanopoulos. J. D. *Rev. Mod. Phys.* **1992**, 64, 1045.

(30) Berendsen, H. J. C.; Postma, J. P. M; van Gunsteren, W. F.; Hermans, J. Interaction models for water in relation to protein hydration. In *Intermolecular Forces*; Pullman, B., Ed.; D. Reidel: Amsterdam, 1981; pp 331.

(31) Teleman, O.; Jonsson, B.; Engstrom, S. *Mol. Phys.* **1987**, 60, 193.

(32) Wallqvist, A.; O Teleman, O. *Mol. Phys.* **1991**, 74, 515.

(33) Smith, D. E.; Haymet, A. D. J. *Fluid Phase Equilib.* **1993**, 88, 79.

(34) Plimpton, S. *J. Comp. Phys.* **1995**, 117, 1.

(35) Hoover, W. G *Phys. Rev. A* **1986**, 34, 2499.

(36) Martyna, G. J.; Tobias, D. J.; Klein, M. L. *J. Chem. Phys.* **1994**, 101, 4177.

(37) Nosé, S. *Mol. Phys.* **1984**, 52, 255.

(38) Hoover, W. G. *Phys. Rev. A* **1985**, 31, 1695.

(39) Verlet, L. *Phys. Rev.* **1967**, 159, 98.

(40) Verlet, L. *Phys. Rev.* **1968**, 165, 201.

(41) Ewald, P. *Annalen der Physik* **1921**, 64, 253.

(42) Rahman, A. *Phys. Rev.* **1964**, 136, A405.

(43) Ohtaki, H; Radnai, T. *Chem. Rev.* **1993**, 93, 1157.

(44) Boyanov, M. I.; Kelly, S. D.; Kemner, K. M.; Bunker, B. A.; Fein, J. B.; Fowle, D. A. *Geochim. Cosmochim. Acta* **2003**, 67, 3299.

(45) Kritayakornupong, C.; Plankensteiner, K.; Rode, B. M. *J. Phys. Chem. A* **2003**, 107, 10330.

(46) Mishra, B.; Haack, E. A.; Maurice, P. A.; Bunker, B. A. *In preparation for Environmental Science and Technology* **2006**.

(47) Hofer, T. S.; Rode, B. M. *J. Chem. Phys.* **2004**, 121, 6406.

**TABLE 1:** Nonbond parameters for the CLAYFF forcefield [5]. The parameters $\varepsilon$ and $\sigma$ determine Lennard-Jones potential well depth and equilibrium distance, respectively.

| **force field type** | **symbol** | **charge (e)** | $\varepsilon$ **(kcal/mol)** | $\sigma$ **(Å)** |
|---|---|---|---|---|
| water hydrogen | h* | 0.410 | | |
| water oxygen | o* | -0.820 | 0.1553999931 | 3.1655413 |
| hydroxyl hydrogen | ho | 0.425 | | |
| hydroxyl oxygen | oh | -0.950 | 0.1553999931 | 3.1655413 |
| bridging oxygen | ob | -1.050 | 0.1553999931 | 3.1655413 |
| tetrahedral silicon | st | 2.100 | 0.0000018405 | 3.3019825 |
| octahedral aluminum | ao | 1.575 | 0.0000013298 | 4.2712536 |
| aqueous chlorine ion | Cl | -1.000 | 0.1001000002 | 4.3999706 |
| aqueous cesium ion | Cs | 1.000 | 0.1000000000 | 3.8310427 |
| aqueous sodium ion | Na | 1.000 | 0.1300999969 | 2.3500126 |
| aqueous cadmium ion | Cd | 2.000 | 0.0470000000 | 2.7627660 |
| aqueous lead ion | Pb | 2.000 | 0.1182000000 | 3.3242995 |

**TABLE 2:** Bond Parameters for the CLAYFF forcefield

| **bond stretch** | | | |
|---|---|---|---|
| **species i** | **species j** | $k_b$ **(kcal/mol Å$^2$)** | $r_o$ **(Å)** |
| o* | h* | 554.1349 | 1.00 |
| oh | ho | 554.1349 | 1.00 |

| **angle bend** | | | | |
|---|---|---|---|---|
| **species i** | **species j** | **species k** | $k_a$ **(kcal/mol rad$^2$)** | $\theta_o$ **(deg)** |
| h* | o* | h* | 45.7696 | 109.47 |

**TABLE 3:** Adsorption statistics calculated from atomic density profiles like those in Figure 5 and Figure 6

| | $Cl^-$ | | | | | | | $Cs^+$ | | | | | | |
|---|---|---|---|---|---|---|---|---|---|---|---|---|---|---|
| | | inner sphere | | | total | | | | inner sphere | | | total | | |
| | $N_{tot}$ | $N_{ad}$ | $X_{ad}$ | $\rho$ | $N_{ad}$ | $X_{ad}$ | $\rho$ | $N_{tot}$ | $N_{ad}$ | $X_{ad}$ | $\rho$ | $N_{ad}$ | $X_{ad}$ | $\rho$ |
| 0.1M | 7 | 3.4 | 49% | 0.09 | 6.6 | 94% | 0.18 | 7 | 4.7 | 66% | 0.12 | 6.6 | 94% | 0.18 |
| 0.5M | 32 | 10.8 | 34% | 0.29 | 17.5 | 55% | 0.47 | 32 | 12.9 | 40% | 0.35 | 19.8 | 62% | 0.53 |
| 1.0M | 64 | 14.7 | 23% | 0.39 | 25.1 | 39% | 0.67 | 64 | 14.3 | 22% | 0.38 | 25.9 | 40% | 0.69 |
| | $Cl^-$ | | | | | | | $Na^+$ | | | | | | |
| | | inner sphere | | | total | | | | inner sphere | | | total | | |
| | $N_{tot}$ | $N_{ad}$ | $X_{ad}$ | $\rho$ | $N_{ad}$ | $X_{ad}$ | $\rho$ | $N_{tot}$ | $N_{ad}$ | $X_{ad}$ | $\rho$ | $N_{ad}$ | $X_{ad}$ | $\rho$ |
| 0.1M | 7 | 3.5 | 50% | 0.09 | 6.1 | 87% | 0.16 | 7 | 0.3 | 4% | 0.01 | 5.3 | 76% | 0.14 |
| 0.5M | 32 | 10.7 | 33% | 0.29 | 20.3 | 64% | 0.54 | 32 | 0.9 | 3% | 0.02 | 12.7 | 40% | 0.34 |
| 1.0M | 64 | 18.8 | 29% | 0.50 | 31.1 | 49% | 0.83 | 64 | 0.7 | 1% | 0.02 | 18.0 | 28% | 0.48 |
| | $Cl^-$ | | | | | | | $Cd^{+2}$ | | | | | | |
| | | inner sphere | | | total | | | | inner sphere | | | total | | |
| | $N_{tot}$ | $N_{ad}$ | $X_{ad}$ | $\rho$ | $N_{ad}$ | $X_{ad}$ | $\rho$ | $N_{tot}$ | $N_{ad}$ | $X_{ad}$ | $\rho$ | $N_{ad}$ | $X_{ad}$ | $\rho$ |
| 0.1M | 14 | 6.1 | 44% | 0.16 | 10.8 | 77% | 0.29 | 7 | 0.0 | 0% | 0.0 | 5.2 | 74% | 0.14 |
| 0.5M | 64 | 12.7 | 20% | 0.34 | 21.2 | 33% | 0.57 | 32 | 0.0 | 0% | 0.0 | 10.3 | 32% | 0.28 |
| 1.0M | 128 | 18.3 | 14% | 0.49 | 28.8 | 23% | 0.77 | 64 | 0.0 | 0% | 0.0 | 11.5 | 18% | 0.31 |
| | $Cl^-$ | | | | | | | $Pb^{+2}$ | | | | | | |
| | | inner sphere | | | total | | | | inner sphere | | | total | | |
| | $N_{tot}$ | $N_{ad}$ | $X_{ad}$ | $\rho$ | $N_{ad}$ | $X_{ad}$ | $\rho$ | $N_{tot}$ | $N_{ad}$ | $X_{ad}$ | $\rho$ | $N_{ad}$ | $X_{ad}$ | $\rho$ |
| 0.1M | 14 | 5.8 | 42% | 0.16 | 10.7 | 76% | 0.28 | 7 | 0.0 | 0% | 0.00 | 6.4 | 91% | 0.17 |
| 0.5M | 64 | 12.9 | 20% | 0.34 | 23.1 | 36% | 0.62 | 32 | 0.0 | 0% | 0.00 | 13.0 | 41% | 0.35 |
| 1.0M | 128 | 17.0 | 13% | 0.45 | 30.1 | 23% | 0.80 | 64 | 0.0 | 0% | 0.00 | 14.1 | 22% | 0.38 |

**TABLE 4:** Solvation and inner sphere adsorption energies for the various cations on the siloxane surface of kaolinite. Uncertainties are ∼4 kcal/mol for all values.

| | **energies (kcal/mol)** | |
|---|---|---|
| **ion** | **solvation** | **adsorption** |
| $Cs^{+}$ | -59 | -74 |
| $Na^{+}$ | -89 | -69 |
| $Cd^{+2}$ | -370 | -100 |
| $Pb^{+2}$ | -313 | -99 |

**TABLE 5:** Coordination numbers (**N**) and characteristic distances (**R**) of aqueous and sorbed complexes. (**exp.**: experimental results; **other MM**: other molecular modeling simulations).

| shell | N | | | R (Å) | | |
|---|---|---|---|---|---|---|
| | **this work** | **exp.** | **other MM** | **this work** | **exp.** | **other MM** |
| **aqueous $Cs^+$** | | | | | | |
| Cs-O* 1st | 8.1 (0.8) | 6-8[a] | 5.3-8.2[a] | 3.12 (0.25) | 2.95-3.21[a] | 3.03-3.20[a] |
| **sorbed $Cs^+$ (inner sphere)** | | | | | | |
| Cs-O* 1st | 5.4 (0.6) | | | 3.12 (0.25) | | |
| Cs-Ob | 5.1 (0.4) | | | 3.41 (0.31) | | |
| Cs-Si | 5.4 (0.4) | | | 4.06 (0.34) | | |
| **aqueous $Na^+$** | | | | | | |
| Na-O* 1st | 5.5 (0.3) | 4-8[a] | 6[a] | 2.37 (0.15) | 2.40-2.50[a] | 2.30-2.40[a] |
| Na-O* 2nd | 16.7 (3.0) | | 12.4[a] | 4.47 (0.57) | | 4.41-4.80[a] |
| **aqueous $Cd^{+2}$** | | | | | | |
| Cd-O* 1st | 7.0 (0.2) | 6[b] | 6[c] | 2.31 (0.11) | 2.27-2.31[b] | 3.33-3.35[c] |
| Cd-O* 2nd | 16.6 (2.0) | 12[a] | 11.7-12.2[c] | 4.59 (0.38) | 4.31-4.37[a] | 4.8-4.9[c] |
| **sorbed $Cd^{+2}$ (outer sphere)** | | | | | | |
| Cd-O* 1st | 7.0 (0.2) | | | 2.31 (0.11) | | |
| Cd-O* 2nd | 13.4 (2.0) | | | 4.57 (0.38) | | |
| Cd-Ob | 6.5 | | | 5.10 | | |
| **aqueous $Pb^{+2}$** | | | | | | |
| Pb-O* 1st | 8.4 (0.2) | 6-11[d] | 8-9[e] | 2.65 (0.13) | 2.45-2.60[d] | 2.60-2.65[e] |
| Pb-O* 2nd | 20.9 (2.0) | | 24[e] | 4.90 (0.40) | | 5.0[e] |
| **sorbed $Pb^{+2}$ (outer sphere)** | | | | | | |
| Pb-O* 1st | 8.4 (0.2) | | | 2.65 (0.13) | | |
| Pb-O* 2nd | 18.1 (2.0) | | | 4.89 (0.42) | | |
| Pb-Ob | 6.5 | | | 5.40 | | |

[a]Ref. [43] [b]Refs. [44, 43] [c]Ref. [45] [d]Ref. [46] [e]Ref. [47]

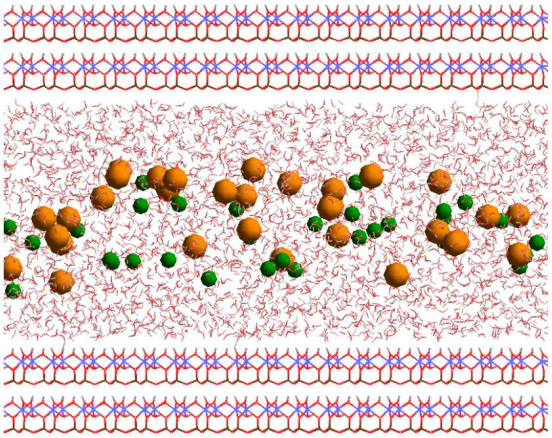

(a) initial configuration

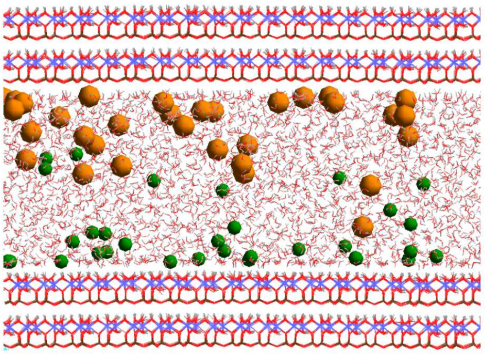

(b) 100 ps

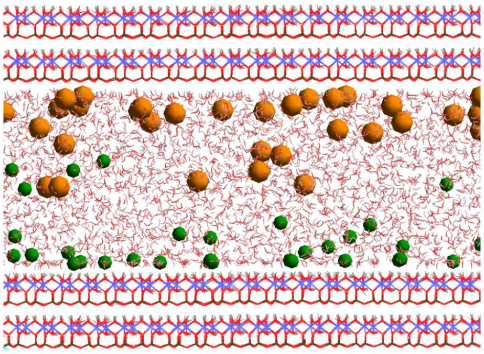

(c) 600 ps

**Figure 1.** Equilibration of a 0.5 M CsCl system. (a) Graphical representation of the initial configuration of the 0.5 M CsCl solution in contact with the basal surfaces of kaolinite; (b) Most of the adsorption has already occurred after 100 ps of dynamics; (c) We run extra 500 ps to assure equilibration. Top and bottom surfaces are the tetrahedral $SiO_4$ and octahedral $AlO_6$ surfaces, respectively. Green and orange balls represent $Cl^-$ and $Cs^+$ ions, respectively.

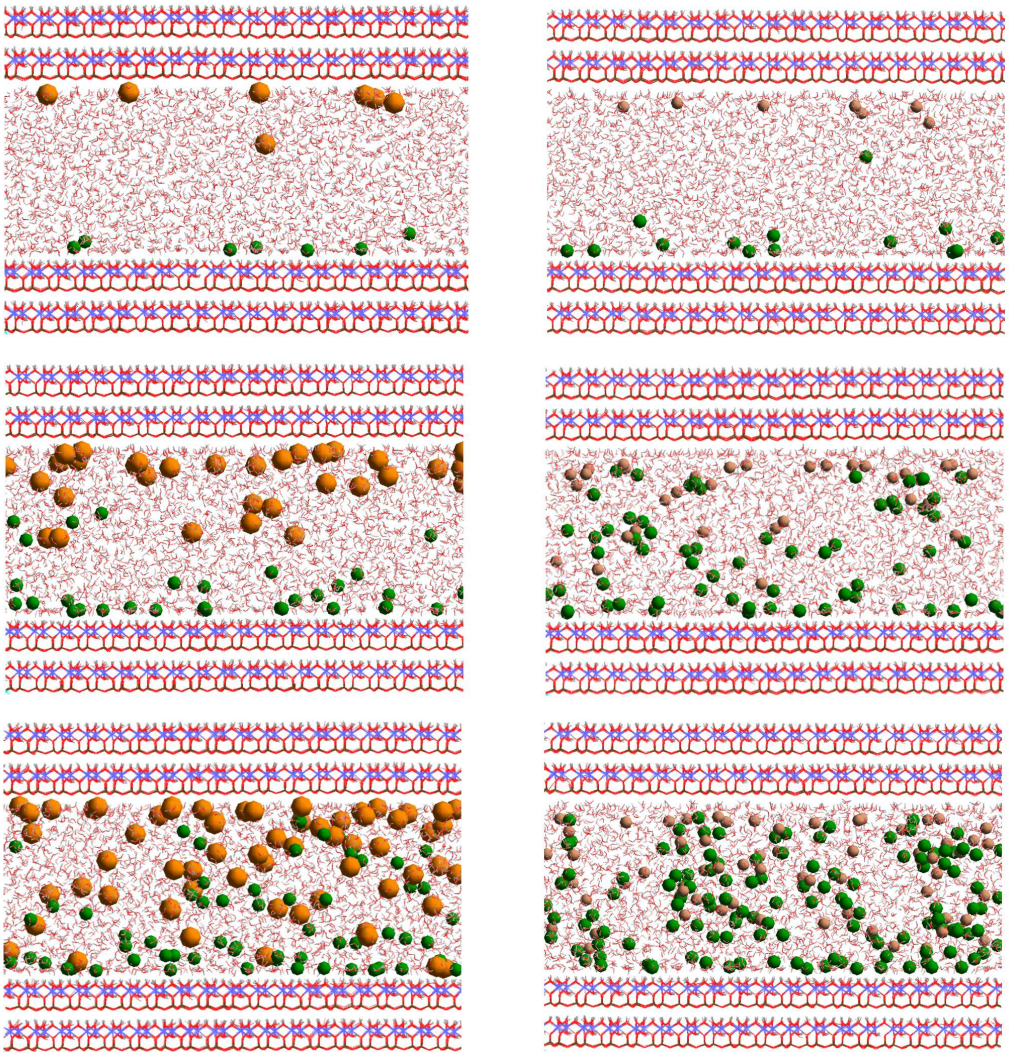

(a) CsCl (b) $CdCl_2$

**Figure 2.** Configurations of each of the three concentrations of CsCl and $CdCl_2$ (0.1 M, 0.5 M, and 1.0 M from the top to the bottom) solutions in equilibrium with the basal surfaces of kaolinite.

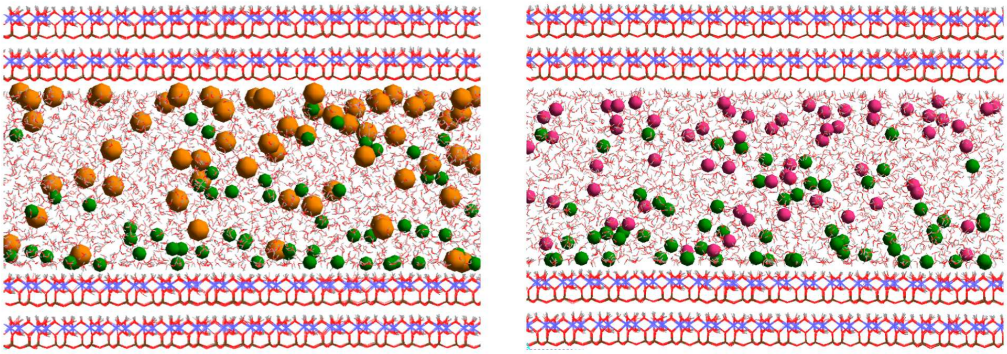

(a) CsCl



(b) NaCl

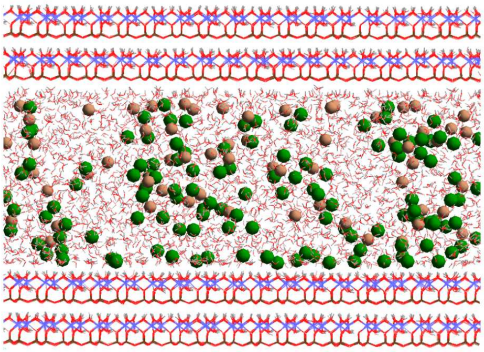

(c) $CdCl_2$

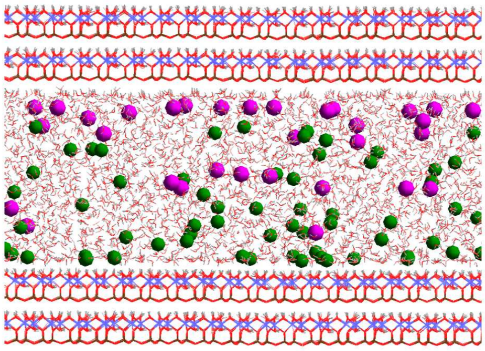

(d) $PbCl_2$

**Figure 3.** Representative configuration of equilibrated 1.0 M solutions in contact with the basal surfaces of kaolinites.

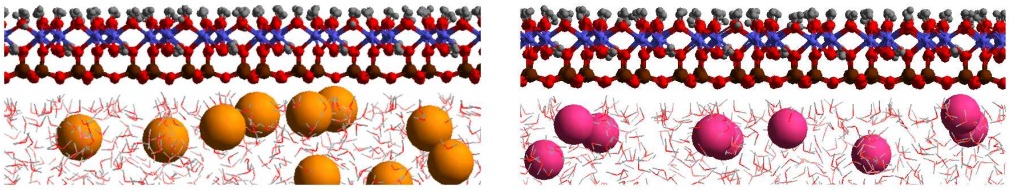

(a) CsCl



(b) NaCl

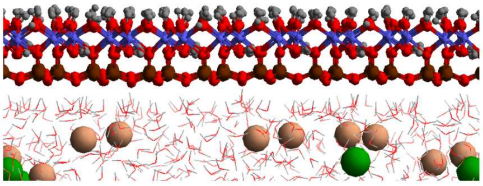

(c) $CdCl_2$

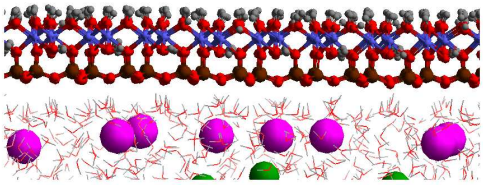

(d) $PbCl_2$

**Figure 4.** Detailed views of the water-kaolinite interface at the $SiO_4$ tetrahedral surface. Notice the predominance of inner sphere adsorption for $Cs^+$, predominance of outer sphere adsorption for $Na^+$, and sole outer sphere adsorption for $Cd^{+2}$ and $Pb^{+2}$.

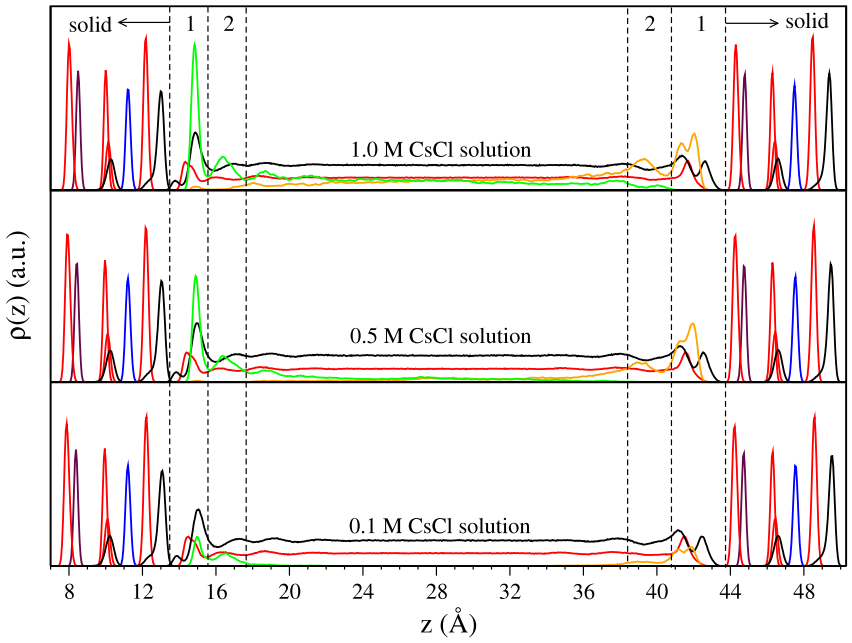


**Figure 5.** Atomic density profiles of the equilibrated 0.1 M, 0.5 M, and 1.0 M CsCl solutions in contact with the two basal surfaces of kaolinite. Colors: Red (O), black (H), blue (Al), maroon (Si), green (Cl), and orange (Cs)

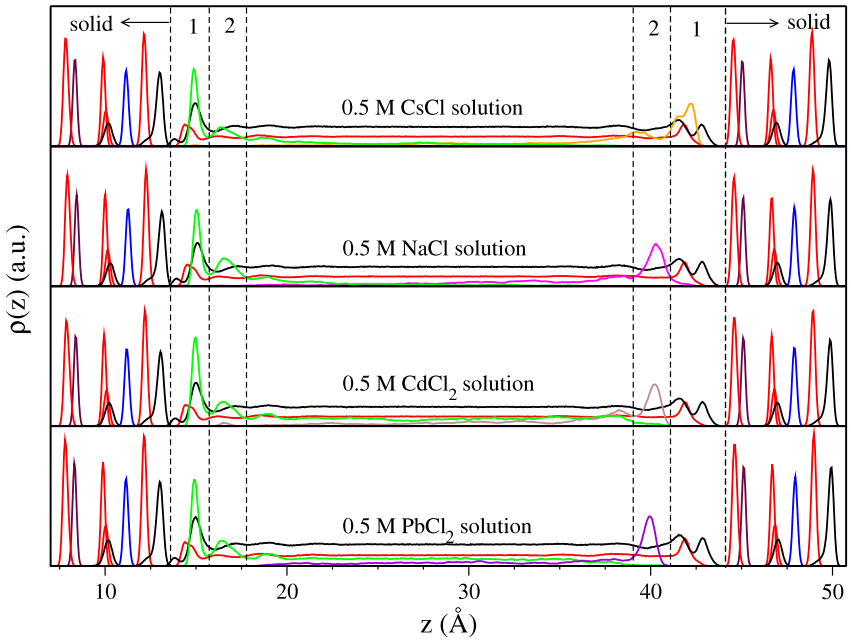


**Figure 6.** Atomic density profiles of the equilibrated 0.5 M solutions in contact with the two basal surfaces of kaolinite. Colors: Red (O), black (H), blue (Al), maroon (Si), green (Cl), orange (Cs), magenta (Na), brown (Cd), and violet (Pb)

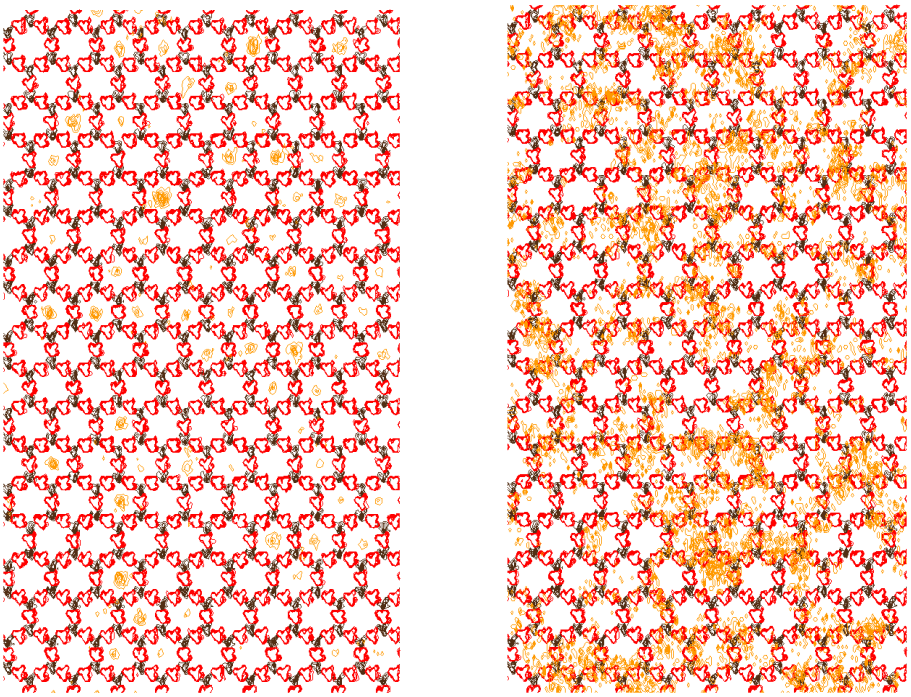

(a) inner sphere (1.0 M CsCl) (b) outer sphere (1.0 M CsCl)

**Figure 7.** Trajectory maps of $Cs^+$ within (a) inner and (b) outer sphere distances to the $SiO_4$ surface, superimposed to the trajectories of silicon and bridging oxygen atoms on the outmost layer of kaolinite. Obtained from the accumulated 500 ps of dynamics. Colors: Red (O), maroon (Si), and orange ($Cs^+$)

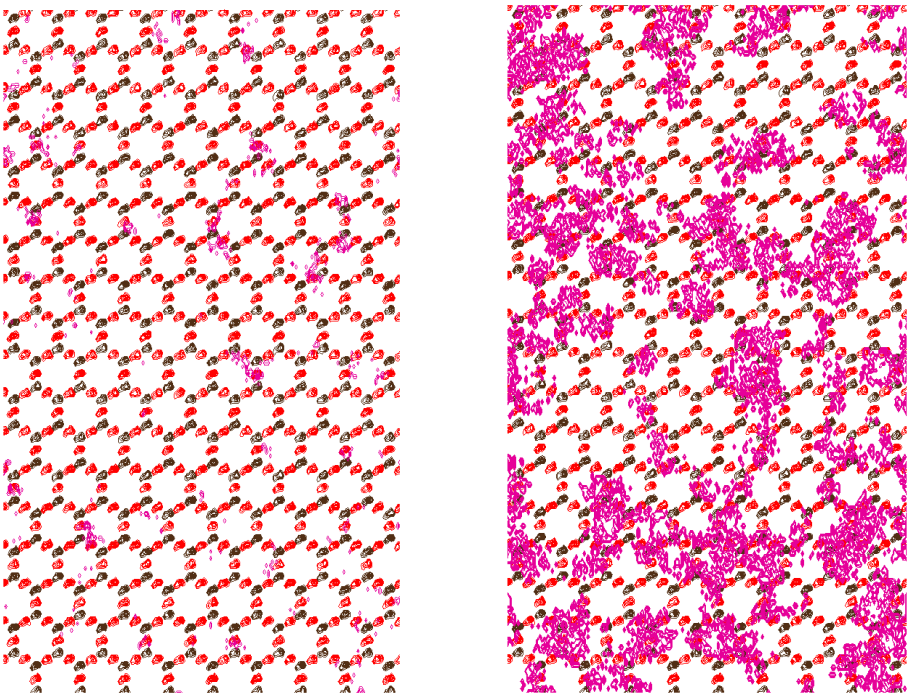

(a) inner sphere (1.0 M NaCl) (b) outer sphere (1.0 M NaCl)

**Figure 8.** Trajectory maps of $Na^+$ within (a) inner and (b) outer sphere distances to the $SiO_4$ surface, superimposed to the trajectories of silicon and bridging oxygen atoms on the outmost layer of kaolinite. Obtained from the accumulated 500 ps of dynamics. Colors: Red (O), maroon (Si), and magenta ($Na^+$).

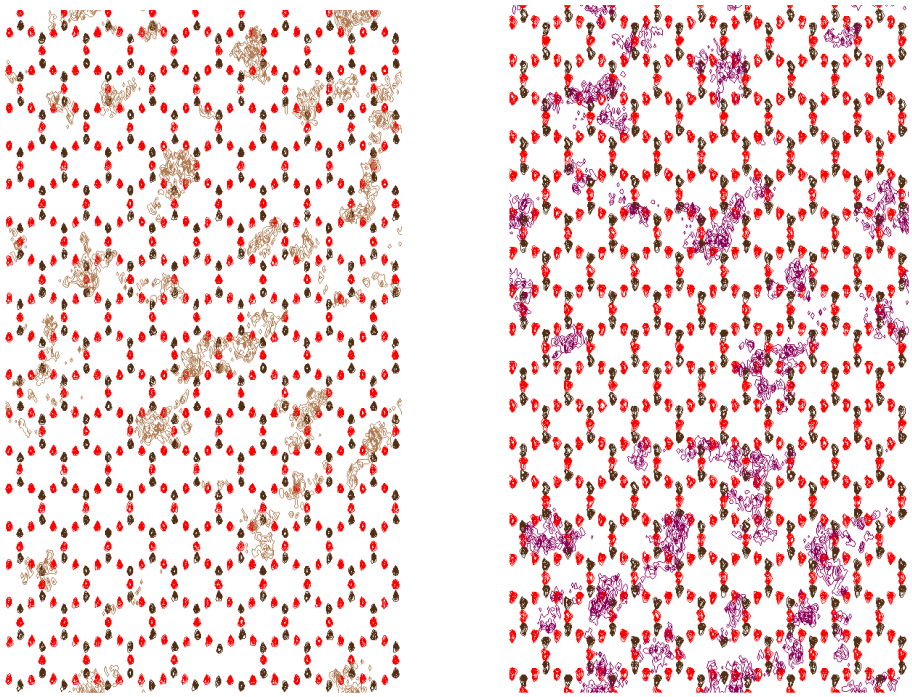

(a) 1.0 M $CdCl_2$ (b) 1.0 M $PbCl_2$

**Figure 9.** Trajectory maps of (a) $Cd^{+2}$ and (b) $Pb^{+2}$ within outer sphere distance to the $SiO_4$ surface, superimposed to the trajectories of silicon and bridging oxygen atoms on the outmost layer of kaolinite. Obtained from the accumulated 500 ps of dynamics. Colors: Red (O), maroon (Al), brown ($Cd^{+2}$), and violet ($Pb^{+2}$)

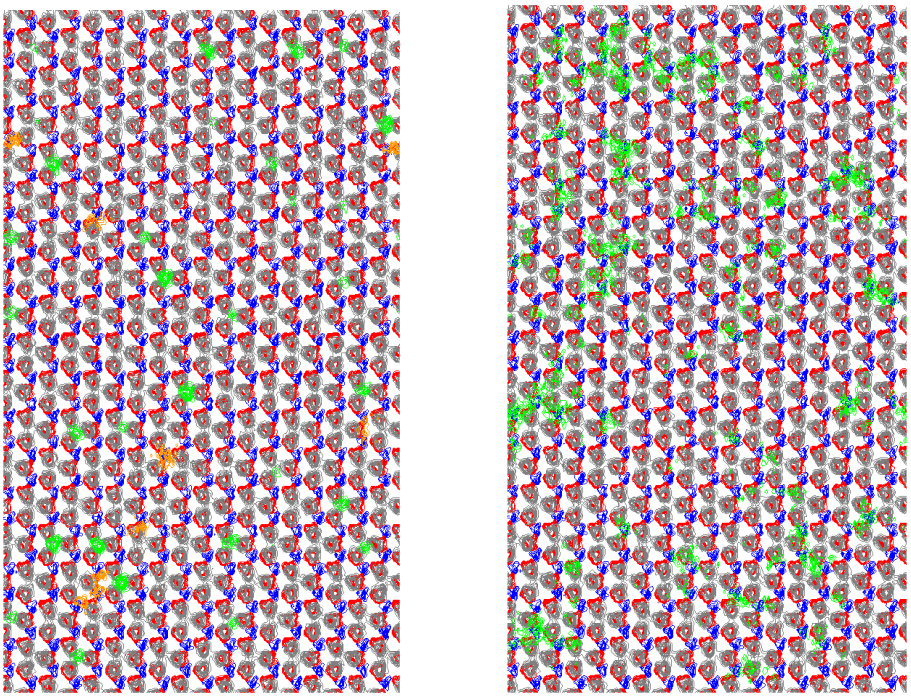

(a) inner sphere (1.0 M CsCl) (b) outer sphere (1.0 M CsCl)

**Figure 10.** Trajectory maps of the 1.0 M CsCl solution in equilibrium with the $AlO_4$ kaolinite surface within (a) inner and (b) outer sphere ranges. Obtained from the accumulated 500 ps of dynamics. Colors: Red (O), black (H), blue (Al), green ($Cl^-$), and orange ($Cs^+$)

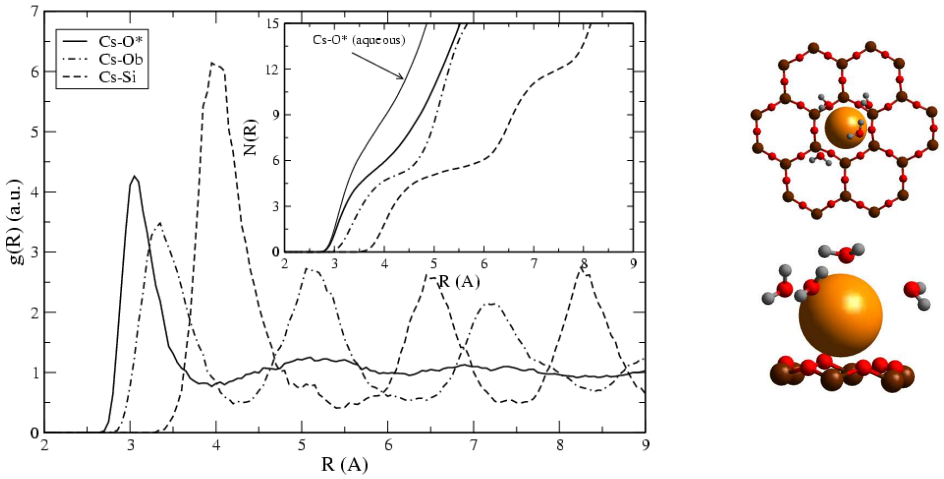


(a) g(R) and N(R)

(b) Adsorption site

**Figure 11.** (a) Radial distribution functions and coordination numbers (detail) for a 0.1 M CsCl solution in equilibrium with kaolinite. (b) Graphical representation of a typical $Cs^+$ adsorption complex.

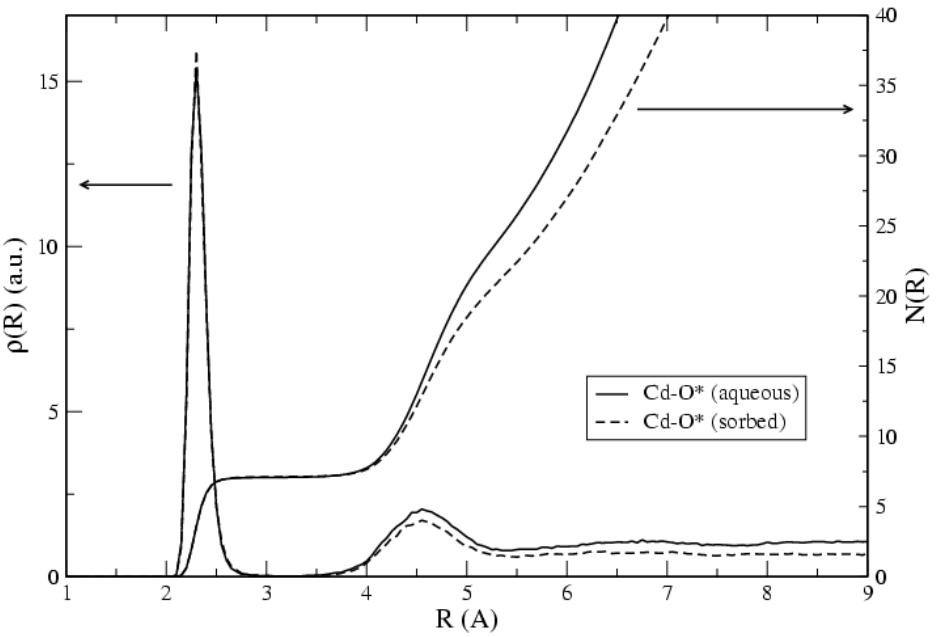


**Figure 12.** Radial distribution functions and coordination numbers calculated from a 0.1 M $CdCl_2$ bulk solution and from a 0.1 M $CdCl_2$ solution in equilibrium with kaolinite.

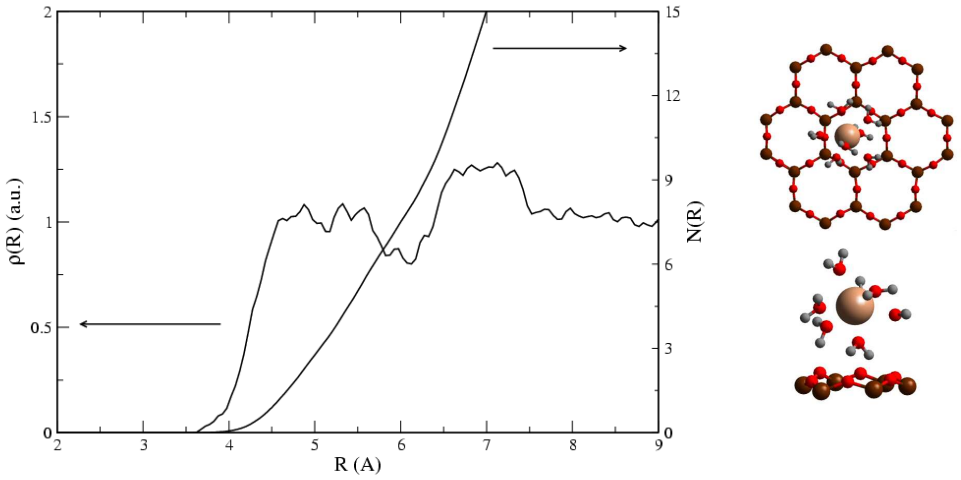


(a) g(R) and N(R)

(b) Adsorption site

**Figure 13.** (a) Cd-Ob radial distribution function and coordination number calculated from a 0.1 M $CdCl_2$ solution in equilibrium with kaolinite. (b) Graphical representation of a typical $Cd^{+2}$ adsorption complex.

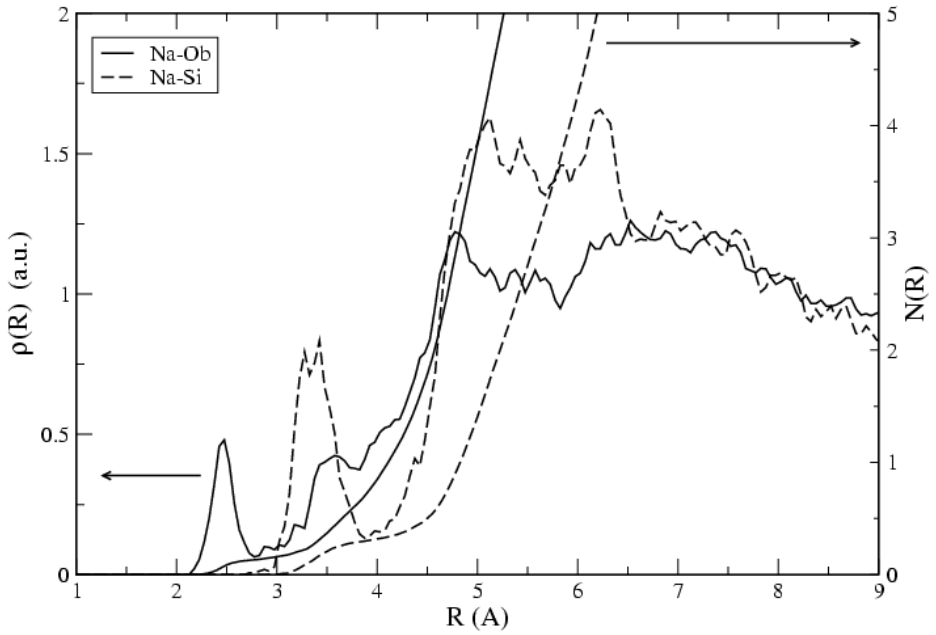


**Figure 14.** Radial distribution functions and coordination numbers for 0.1 M NaCl solution in equilibrium with kaolinite.